Radiation from free electrons in a laser focus at 10^{18} W/cm^2: modeling of photon yields and required focal conditions

Grayson Tarbox,[1] Eric Cunningham,[1] Ryan Sandberg,[1] Justin Peatross,[1,2] and Michael Ware[1,*]

[1]*Dept. of Physics and Astronomy, Brigham Young University, Provo, Utah 84602, USA*
[2]*e-mail: peat@byu.edu*
**Corresponding author: ware@byu.edu*

Received December 23, 2014; revised February 11, 2015; accepted February 13, 2015;
posted February 18, 2015 (Doc. ID 231361); published April 8, 2015

In support of an experiment designed to measure the strength of radiation scattered from low-density free electrons in an intense laser focus, we model a variety of physical parameters that impact the rate of scattered photons. We employ a classical model to characterize duration of electron exposure to high-intensity laser light in a situation where the electrons are driven by strong ponderomotive gradients. Free electrons are modeled as being donated by low-density helium, which undergoes strong-field ionization early in the pulse or during a prepulse. When exposed to relativistic intensities, free electrons experience a Lorentz drift that causes redshifting of the scattered 800 nm light. This redshift can be used as a signature to discern light scattered from the more intense regions of the focus. We characterize the focal volume of initial positions leading to significant redshifting, given a peak intensity of 2×10^{18} W/cm^2. Under this scenario, the beam waist needs to be larger than several wavelengths for a pulse duration of 35 fs. We compute the rate of redshifted scattered photons from an ensemble of electrons distributed throughout the focus and relate the result to the scattered-photon rate of a single electron. We also estimate to what extent the ionization process may produce unwanted light in the redshifted spectral region.

OCIS codes: (000.1600) Classical and quantum physics; (270.5580) Quantum electrodynamics; (290.5820) Scattering measurements; (350.5720) Relativity.
http://dx.doi.org/10.1364/JOSAB.32.000743

1. INTRODUCTION

Free electrons in a laser focus undergo relativistic motion at optical frequencies for laser intensities around and above 10^{18} W/cm^2. The availability of relativistic intensities during the past two decades has spurred a number of investigations into electron behavior in such a laser focus, including ponderomotive acceleration, Lorentz drift, and plasma wakefield generation [1–6]. Thomson scattering from relativistically excited plasmas has also been studied [7,8]. Meanwhile, theoretical investigations into the dynamics of individual free electrons in intense laser fields have been pursued [9–11] together with the study of the associated scattered radiation [12–15].

In the ionization process, an electron wave function typically is initially localized in both momentum and position, but can quickly spread to become comparable in size to the wavelength of the driving field. This is especially true if the wave function ionizes over several laser cycles [13]. It is interesting to consider how a large electron wave packet scatters radiation when different parts of the same wave function oscillate out of phase in the driving laser field. Quantum electrodynamics (QED) predicts that an electron radiates with the strength of a point emitter, regardless of the spatial extent of its wave packet [16,17]. This is in contrast with a first-quantized picture where one might intuitively expect that radiation from a single large electron wave packet undergoes interference and suppression [18].

We are conducting an experiment to measure the radiation from free electron wave packets to effectively test the QED prediction. Whereas QED predicts that light scattering is independent of wave packet size, the first-quantized picture would predict suppression by typically two orders of magnitude in a direction perpendicular to laser propagation, so long as the quantum electron wave packet is treated as a classical light source and it extends over a distance of a laser wavelength or greater [15].

In the experiment, we backfill helium into an evacuated chamber wherein a high-intensity laser pulse is focused. The laser pulse can easily liberate both electrons from any helium atom that happens to be located within the focus. Depending on the exact location of a particular electron-donor atom, the liberated electrons may undergo relativistic motion. The Lorentz drift of such electrons causes laser light scattered out the side of the focus to be redshifted in comparison to the driving laser. This redshift is convenient for an experiment seeking to spectrally discriminate between photons scattered from free electrons and other possible noise sources.

In this paper, we present simulations of relativistic electron behavior in a laser focus. This information will be important for the interpretation of data collected in an experimental setup outlined in Section 2. Section 3 describes a simple model of light emission based on a classical point electron, which radiates with a strength similar to QED predictions. In Section 4, we characterize the amount of redshift in the

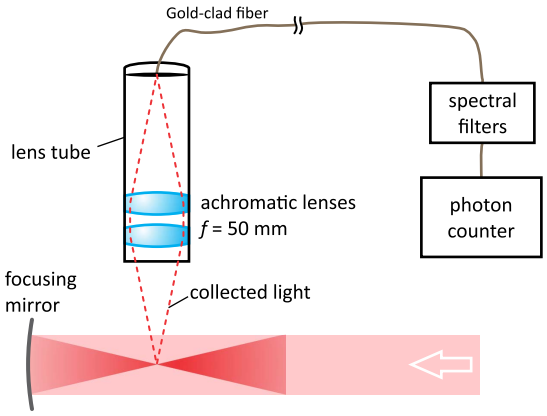

Fig. 1. Schematic of the experiment showing the one-to-one imaging system used to collect redshifted photons scattered from free electrons in a laser focus.

perpendicularly scattered radiation as a function of laser intensity. In Section 5, we characterize the effective volume within the focus wherein the scattered radiation is significantly redshifted. In Section 6, we comment on the emission from a large ensemble of free electrons, emphasizing the well-known fact that, in the direction perpendicular to the laser propagation, the scattered light should be proportional to the number of ensemble members. Since each helium atom donates a pair of electrons, we consider in Section 7 the correlation between electron trajectories as well as the rate of wave packet spreading in the laser field. In Section 8, we estimate of the strength of light emission from electrons during the ionization process and subsequent collisions. Finally, in Section 10, we calculate predicted signal levels for the experimental setup.

2. EXPERIMENTAL SETUP

The basic layout of the experiment is shown in Fig. 1. A Ti:sapphire laser system produces 800 nm, 35 fs laser pulses, which are focused by an on-axis elliptical mirror to intensities in the 2×10^{18} W/cm^2 range. The interaction chamber is evacuated to $<10^{-8}$ Torr and then backfilled with helium, which donates free electrons through ionization. With each laser pulse, helium atoms in the laser focus become doubly ionized, and their electrons are accelerated in the intense laser field, causing them to radiate. A lens collects light emitted out the side of the laser focus using a one-to-one imaging system, which subtends approximately 0.2 sr in the proposed experiment. The collected photons are coupled into a gold-clad multimode fiber and routed to a single-photon detection system.

The relativistic intensity experienced by the free electrons not only increases the scattering rate, but also causes the electrons in the most intense part of the focus to drift forward at a significant fraction of the speed of light, owing to the Lorentz force $e\mathbf{v} \times \mathbf{B}_L$. This forward velocity causes the photons scattered out the side of the focus to be redshifted relative to the laser. Spectral filtering (using a 875–925 nm bandpass filter in our case) can discriminate for these redshifted photons, which originate in a quantifiable volume within the laser focus. The photons of interest also arrive within a specific time window, which further helps to differentiate them (with 0.1 ns instrument resolution) from other potential noise sources such as light scattered from the chamber wall. These filtering techniques allow individual scattering events to be distinguished from the sea of 10^{17} photons in each laser pulse.

3. COMPUTATIONAL MODEL

Simulating the quantum dynamics of a free electron in a laser focus is a numerically intensive endeavor [19,20]. To make the calculation more manageable, Chowdhury *et al.* used a hybrid quantum/classical model [13]. First, a tunneling-ionization rate model was used to promote an increasing fraction of the electron probability into the continuum. Once in the continuum, each tiny portion of the wave packet was propagated as a classical point-like trajectory. Many point-like elements taken together represented the free electron wave, and the different elements spread out under the influence of the strong laser field. This approach is reasonable since typical quantum forces in this case are tiny in comparison to the extreme forces of the laser field.

We essentially take the approach outlined by Chowdhury *et al.*, except we represent an electron with just a single classical point-like trajectory driven in the laser focus. The single classical point-like trajectory offers a strength of emission consistent with the QED prediction. Since the experiment seeks to distinguish scattering strengths that differ by two orders of magnitude, an analysis based on a point electron is sufficient for estimating a photon-scattering rate consistent with QED. A much lower scattering rate would align with the first-quantized viewpoint, where emission from different pieces of a large electron wave packet is allowed to interfere.

We employ classical electrodynamics to simulate the interaction of the laser field with the electron. The lab-frame acceleration of an electron in the presence of electric and magnetic fields is given (in MKS units) by the well-known formula [21]

$$\mathbf{a} = -\frac{e}{\gamma m}\left[\mathbf{E}_L + \mathbf{v} \times \mathbf{B}_L - \frac{\mathbf{v}(\mathbf{v} \cdot \mathbf{E}_L)}{c^2}\right], \tag{1}$$

where e, m, and $\mathbf{v}$ are the charge, mass, and velocity of the electron, respectively, $\gamma = 1/\sqrt{1 - v^2/c^2}$ is the usual relativistic factor, and $\mathbf{E}_L$ and $\mathbf{B}_L$ are the electric and magnetic fields of the laser, respectively. We integrate Eq. (1) using fourth-order Runge–Kutta to calculate the electron trajectories for various initial conditions.

In the far field, the radiation scattered by an electron to a measurement point $(\mathbf{r}, t)$ can be calculated as

$$\mathbf{E}(\mathbf{r}, t) = \frac{q}{4\pi\varepsilon_0 \imath}\frac{\hat{\boldsymbol{\imath}} \times (\mathbf{u} \times \mathbf{a})}{(\hat{\boldsymbol{\imath}} \cdot \mathbf{u})^3} \quad \text{and} \quad \mathbf{B} = \frac{1}{c}\hat{\boldsymbol{\imath}} \times \mathbf{E}, \tag{2}$$

where $\mathbf{u} \equiv c\hat{\boldsymbol{\imath}} - \mathbf{v}$ and $\boldsymbol{\imath} \equiv \mathbf{r} - \mathbf{r}'$. Here, $\mathbf{r}'$ is the position of the electron at the retarded time t_r, given implicitly by $\imath = c(t - t_r)$. The electron acceleration $\mathbf{a}$ and velocity $\mathbf{v}$ are similarly evaluated at t_r. We neglect the self force of the electron due to scattered radiation; the self force is approximately seven orders of magnitude below the force of the laser field in our regime. The spectrum of the scattered light at a given location and for a specific laser field is found by Fourier transforming the fields in Eq. (2).

4. TARGET PEAK INTENSITY

We first use our computational model to study the radiation from free electrons beginning at rest as a function of the peak

intensity of the laser pulse. To remove spatial effects due to focusing, we here consider a linearly polarized plane-wave pulse propagating in the z dimension (extending infinitely in the x and y dimensions) having a Gaussian temporal envelope with duration 35 fs (FWHM). Figure 2(a) shows several transverse oscillations of a free electron interacting with this plane-wave pulse near its peak at a variety of peak intensities. The period of the oscillations increases to the extent that the Lorentz drift causes the electron to move with the laser pulse at a significant fraction of c. As the intensity increases into the relativistic regime, the oscillation frequency is significantly redshifted.

Figure 2(b) shows the trajectory taken by an electron as it interacts with a pulse with peak intensity 2×10^{18} W/cm^2. During the course of the pulse, the electron drifts forward a little more than three laser wavelengths and undergoes nonlinear motion before eventually coming to rest again. Figure 2(c) shows the far-field intensity spectrum computed via Eq. (2) for the various electron trajectories associated with pulses of different peak intensities. The spectra are calculated for a detector located in the direction perpendicular to both the pulse-propagation direction and the direction of the linear polarization. The spectrum undergoes an increasing amount of redshift (and stronger emission) as the light pulse intensity increases. At the lowest intensity shown, $I_0 = 1 \times 10^{17}$ W/cm^2, the spectrum resembles that of the incident light pulse, being only slightly redshifted from the original spectral center of 800 nm. The intensity $I_0 = 1.5 \times 10^{18}$ W/cm^2 gives an amount of redshift ideal for our experiment, which keys in on the spectral window 875–925 nm. This window gives sufficient separation from the laser spectrum while still maintaining a suitable detection efficiency using a silicon avalanche photodiode.

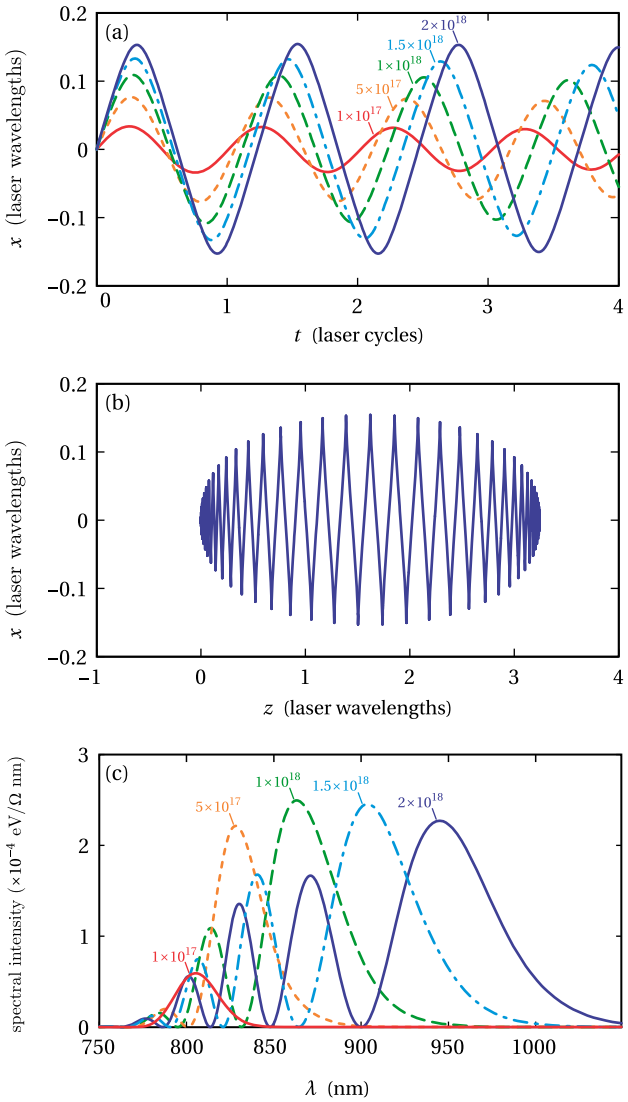

Fig. 2. (a) Oscillations of an electron near the peak of a plane-wave pulse with a Gaussian temporal window (FWHM 35 fs) and $\lambda_L = 800$ nm. The phases of oscillation associated with the different peak intensities are shifted to align at $t = 0$ for easier comparison. (b) Trajectory of an electron experiencing the pulse with peak intensity $I_0 = 2 \times 10^{18}$ W/cm^2. (c) Far-field radiation spectrum, in the direction perpendicular to both the pulse propagation and to the linear polarization, generated by a free electron experiencing the various plane-wave pulses in (a).

5. BEAM WAIST CONSTRAINTS

Finite laser pulse energy necessitates a tight focus to achieve relativistic intensities. Electrons in a tightly focused laser experience strong ponderomotive gradients that can cause them to leave out the side of the focus before the peak of the pulse arrives. The more tightly focused a laser beam, the stronger the gradient and the shorter the distance for the electron to escape from the high-intensity region. Thus, we need to characterize how tight the focus can be while still allowing the electrons sufficient time in the high-intensity region.

To model the laser focus, we employ a single-frequency representation for the vector fields of the laser focus according to Salamin *et al.* [1] and append *ad hoc* a moving time envelope with wavefront curvature to form the laser pulse (as opposed to the more correct superposition of a range of single-frequency solutions). For these simulations, we fix the peak intensity at $I_0 = 2 \times 10^{18}$ W/cm^2 with pulse duration 35 fs FWHM. For these parameters, the laser focus experiences about 10 laser cycles above 1.5×10^{18} W/cm^2 at the origin. This parameter set matches pulses available in our laboratory.

Figure 3 shows 20 distinct electron trajectories originating from random positions within the more intense region of the laser focus with a beam waist $w_0 = \lambda_L$. The electrons depicted in Fig. 3 leave the tight laser focus quickly, experiencing a maximum intensity typically a factor of 5 below the peak of 2×10^{18} W/cm^2. This extremely tight focus is clearly too small for the proposed experiment. In this section, we explore how loose the focus needs to be for thorough exposure of ionized electrons to the highest intensities.

To characterize the volume of the region wherein the electron's initial position gives rise to a trajectory that experiences relativistic intensities for suitable duration, we release electrons from various initial positions in the focus and compute their trajectories under the influence of the laser field. Figure 4 plots the average length of time that a free electron experiences an intensity above 1.5×10^{18} W/cm^2 as a function of beam waist w_0 and initial position x_0, y_0, and z_0. When generating these plots, the electron is released from rest when the laser field first exceeds the threshold for second ionization of helium (corresponding to $I = 8.7 \times 10^{15}$ W/cm^2) at the initial position. The carrier-envelope phase of the laser can significantly alter the time spent in the high-intensity region, so

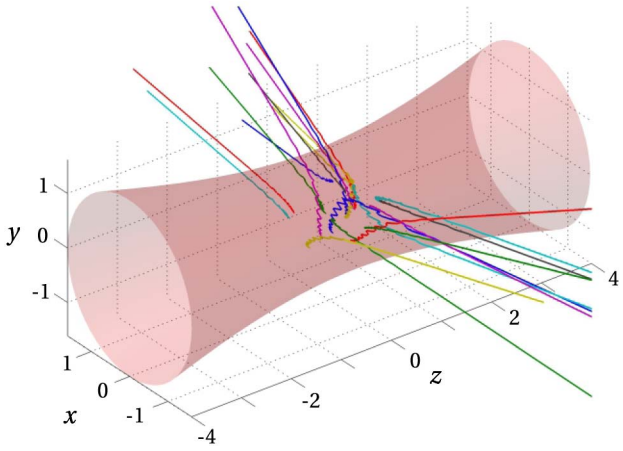

Fig. 3. Simulated trajectories of 20 electrons born in a laser pulse focused with waist $w_0 = \lambda$. The laser has peak intensity 2×10^{18} W/cm^2 and duration 35 fs. The electron initial positions are randomly distributed within the volume where the intensity is above 1×10^{18} W/cm^2.

the plots are averaged over carrier envelope phase, which smooths out this effect.

Figure 4(a) plots the duration of exposure to high intensity for an electron originating from various values of x_0 along the line $y_0 = 0, z_0 = 0$. Figure 4(b) similarly shows the duration of exposure if the electron originates from various y_0 positions on the line $x_0 = 0, z_0 = 0$. The laser pulse is linearly polarized in the x direction. At larger beam waists, an electron near the center experiences the maximum 10 cycles of high intensity. If the beam waist narrows to less than about $3\lambda_L$, the range of positions that experience this high intensity for any amount of time quickly goes to zero. In this case, the electron is typically

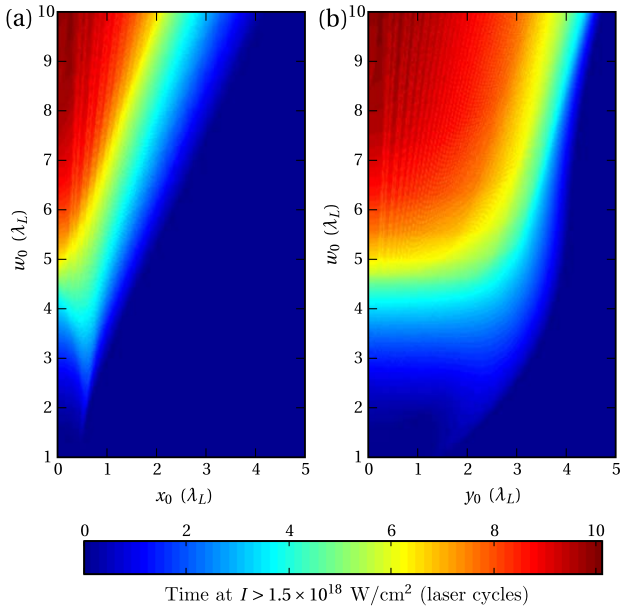

Fig. 4. Time an electron experiences $\geq 1.5 \times 10^{18}$ W/cm^2 plotted against the beam waist w_0 and the initial position. The electron is released when the intensity first crosses the second ionization threshold of helium. The peak intensity of the pulse is held at $I_0 = 2 \times 10^{18}$ W/cm^2 and duration 35 fs FWHM. In (a) the initial position is $y_0 = 0, z_0 = 0$, and x_0 is varied. In (b) the initial position is $x_0 = 0, z_0 = 0$, and y_0 is varied.

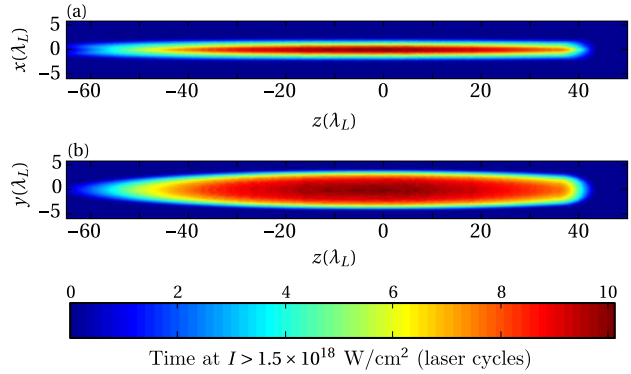

Fig. 5. Two-dimensional slices, (a) x–z and (b) y–z planes, depicting the time an average electron experiences intensities above 1.5×10^{18} W/cm^2 plotted versus its initial position. The pulse parameters were chosen to be $I_{\text{peak}} = 2 \times 10^{18}$ W/cm^2, $w_0 = 6\lambda_L$, $\lambda_L = 800$ nm, and $\tau_L = 35$ fs (FWHM).

pushed out of the high-intensity region before the highest intensity portion of the pulse arrives. Our laser system has sufficient pulse energy to achieve the peak intensity of $I_0 = 2 \times 10^{18}$ W/cm^2 for a beam waist of $w_0 \approx 6\lambda_L$, given a 35 fs pulse duration. To expose electrons to these intensities for significantly longer times would require either a wider focus or a special ponderomotive trapping scheme such as developed by Chaloupka *et al.* [22].

To estimate the volume wherein electrons experience high intensity for significant time, we ran simulations with electrons starting from a variety of initial positions in a laser focus. Figure 5 depicts horizontal and vertical cross sections of the volume wherein the initial position enables an electron to experience an intensity above 1.5×10^{18} W/cm^2. The color coding indicates the amount of time the average electron experiences above that intensity. For comparison, the laser intensity reaches 1.5×10^{18} W/cm^2 within a radius of $\sqrt{x^2 + y^2} = 0.38 w_0$ and within a longitudinal range of $|z| < 82\lambda_L$, which constitutes about six times the effective volume depicted in Fig. 5. Since electrons drift in the forward direction, the range of initial positions before the focus that experience long times at high intensity is larger than the range of positions after the focus. Since the linear polarization is in the x direction, initial positions that are offset from the axis in y experience the high intensity for a longer duration than initial positions that are similarly offset in x.

6. SIGNAL SCALING WITH NUMBER OF ELECTRONS

Given the low photon-scattering rate seen in Fig. 2 and the limited practical detector efficiency, it is clear that any feasible experiment needs to employ many electrons simultaneously in the focus. The electrons of interest need to be confined to the small region of high intensity discussed in the previous section, so we need to understand how emissions from neighboring electrons interact. In this section, we consider how the radiation signal scales with electron number and density.

The trajectories of two electrons released from the same helium atom are initially correlated, and the electron pair radiates coherently for a factor of 2 increase in signal. However, as discussed in the next section, we plan to pre-ionize the

helium and allow some spreading and separation before the primary high-intensity laser pulse arrives. Thus, we expect this enhancement to be small and have not included it in the signal plots below.

For electrons from separate atoms, the emission directed perpendicular to the laser propagation is incoherent if the electrons are distributed randomly throughout the focus. Although there is a coherent buildup of emission in the forward direction, phase matching in the perpendicular direction is sufficiently poor to avoid coherent effects (other than between electron pairs released from the same atom). That is, the phases of emission from the various electrons may be treated as random by virtue of the random locations within the focus. In this case, the emission intensities calculated for the individual electrons released from different atoms sum on average.

To confirm this intensity-addition rule (in the perpendicular direction), we computed emission from many electron pairs released from atoms randomly positioned throughout the focus. As expected, we find that the emission indeed fluctuates around an intensity equal to the single-atom intensity multiplied by the number of atoms. Thus, it is straightforward to connect emission behavior from many free electrons to the single-electron behavior we desire. However, we do need to ensure that densities remain sufficiently low so as to avoid cooperative effects (i.e., keeping electron spacing greater than a half wavelength) [23]. This limits the donor-atom pressure to below about 10^{-4} Torr.

7. IONIZATION AND SPREADING

There are no atoms that will donate only a single electron in the presence of the laser intensities considered here. Hydrogen is found naturally in a diatomic state, and it is reactive in its monatomic state. Helium is inert and has just two electrons, making it our donor atom of choice. Conveniently, the electrons of helium ionize at a higher intensity than the first two electrons from any other atom or molecule.

For our purposes, we use a simple over-the-barrier ionization model to estimate the intensities necessary to ionize helium: 1.3×10^{15} W/cm^2 for single ionization and 8.7×10^{15} W/cm^2 for double ionization [24]. Figure 6 depicts the focal regions where first and second ionization of helium takes place. The ionization volumes are, respectively, about 10^5 and 10^4 times larger than the tiny high-intensity volume depicted in Fig. 5.

Since the two electrons are released at different intensities and potentially at different laser oscillation phases, their subsequent trajectories tend to separate somewhat. Ionization at these intensities can result in drift velocities of $v = 0.007\,\frac{\mu m}{fs}\,\sin\phi$ and $v = 0.019\,\frac{\mu m}{fs}\,\sin\phi$, respectively, where ϕ represents the laser phase upon release (with $\phi = 0$ corresponding to the peak of the field). A reasonable range for the laser phase upon release is $\phi = \pm\pi/6$, which translates into drift-velocity ranges of $v = \pm0.004\,\frac{\mu m}{fs}$ and $v = \pm0.010\,\frac{\mu m}{fs}$ along the direction of polarization. Given these relatively modest velocities, the trajectories of electron pairs from doubly ionized helium tend to remain correlated in the laser field over several tens of femtoseconds. They typically separate by more than a wavelength if the timescale exceeds hundreds of femtoseconds.

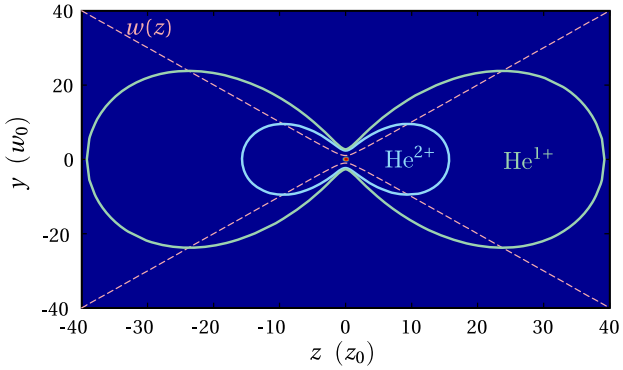

Fig. 6. Cross section of the laser focus (side profile) showing regions of first and second ionization of helium as well as the comparatively tiny high-intensity region from Fig. 5(b), where free electrons experience high intensity and emission is redshifted. The laser parameters are the same as in Fig. 5.

The quantum spreading of electrons is another relevant consideration. As an electron undergoes ionization over several laser cycles, a fraction of the wave function bleeds away near the peak of each oscillation over a range of phases ϕ. Thus, different pieces of the same wave packet are launched with different drift velocities, much as in the above discussion regarding the two different helium electrons. That is, the electron wave functions each end up incorporating the full available range of phases. Moreover, natural quantum spreading for a free wave packet initially the size of a helium atom spreads (via the uncertainty principle) at a rate of $\pm0.003\,\frac{\mu m}{fs}$, which is remarkably on par with the spreading due to the variety of release phases. Since the goal of our experimental effort is to measure photon scattering from large electrons, a prepulse can be used, arriving 100–200 fs prior to the main relativistic laser pulse, to give the free electron wave packets time to spread to the scale of a laser wavelength.

The question of whether electron pairs from the same helium atom remain correlated only impacts the rate of scattered radiation by a factor of 2. On the other hand, the first-quantized and QED viewpoints of large wave packets predict different signals by two or more orders of magnitude.

8. RADIATION FROM THE IONIZATION PROCESS

In this section, we consider the level of photoemission that might arise during the ionization process. To estimate the strength of this potential noise source, we simulated the ionization process of helium using a pair of classical electrons caught in a smoothed Coulomb potential well, subject to the oscillating laser field. This model, used by Ho and coworkers [25], allows the electrons to naturally break free from the core at the appropriate intensities and to interact with the long-range Coulomb tail of the parent ion while oscillating in the field. We use Eq. (2) to estimate the electron radiation, both before and after each electron detaches from the core, while still under the influence of the Coulomb potential.

Using this model, we find that any spectral components overlapping the redshifted bandpass region arise almost entirely from the fact that the electron suddenly breaks free

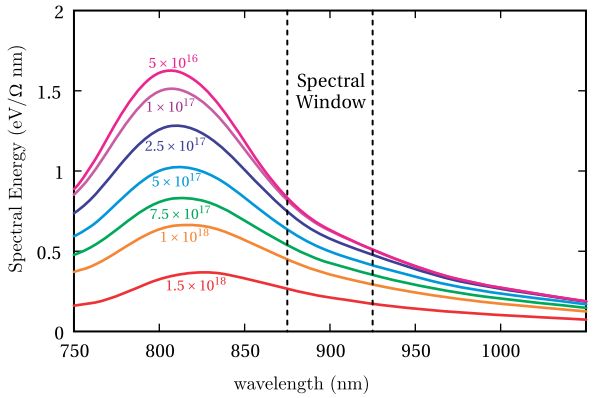

Fig. 7. Total energy per shot for randomly distributed electrons within the entire ionization volume with a density appropriate for a pressure of 5×10^{-5} Torr. The different curves represent the radiation from the set of electrons that experience at least one cycle at an intensity of 15×, 10×, 7.5×, 5×, 2.5×, 1×, or 0.5×10^{17} W/cm^2. The laser parameters are the same as those for Fig. 5, with peak intensity 2×10^{18} W/cm^2. The spectrum is measured in the far field in a direction perpendicular to the direction of laser propagation and to the direction of linear laser polarization.

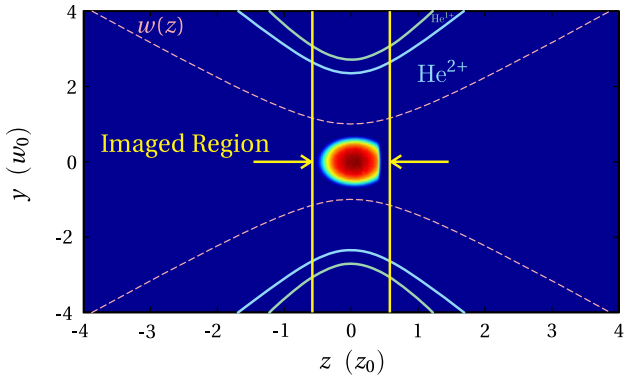

Fig. 8. Zoomed-in portion of Fig. 6 showing the small region of the focus that is imaged into the fiber.

of the nucleus, without regard to any specific features in the electron trajectory as it exits the atom. One obtains essentially the same result by simply releasing the electron from rest, once the local electric field reaches the appropriate strength. The abrupt initiation of oscillations (on the time scale of a laser period) leads to faint spectral wings, independent of the details of the model that does the releasing. This effect is similar (although reversed in time) to spectral wings observed in instantaneous spectra, computed in a different context [26]. In any case, the spectral wings overlapping the redshifted region of interest are approximately three orders of magnitude smaller than the redshifted signal emitted by the electrons that experience 1.5×10^{18} W/cm^2. Still, because the volume undergoing ionization is enormous compared to the relevant high-intensity region, it becomes necessary to cut out most of the ionization volume, as will be discussed in Section 10.

9. REDSHIFT VERSUS INTENSITY

To estimate the overall signal coming from the focal volume, we calculated the expected emission from a group of free electrons with random initial positions within the double ionization region of the focus depicted in Fig. 6. The laser parameters were kept the same as in Fig. 5 for this simulation. We averaged a large number of intensity spectra, generated from randomly chosen individual electron trajectories, and then scaled the resulting spectrum to be representative of the total signal per laser shot at a density associated with a helium pressure of 5×10^{-5} Torr (involving about 35,000 electrons). We ignore any possible collisions between electrons and neighboring ions. The result is shown in Fig. 7. Several curves are shown for partial volumes wherein the electrons experience at least one oscillation at the various threshold intensities. Notice that as the threshold intensity for inclusion is reduced below 1×10^{17} W/cm^2, the signal in the 875–900 nm range does not significantly increase.

While the distinct spectral structures seen in Fig. 2 wash out in Fig. 7, a strong redshift from the laser wavelength 800 nm is apparent. Based on Fig. 7 and assuming a 0.2 steradian collection angle, a 875–925 nm bandpass filter, a 5% detector efficiency, and a pressure of 5×10^{-5} Torr, one arrives at $0.7 \frac{\text{eV}}{\Omega \cdot \text{nm}} \times 50 \text{ nm} \times 0.2\ \Omega \times 0.05 = 0.3$ eV per shot, or about one photon per 5 shots emitted from the entire ionization volume.

10. EXPERIMENTAL SIMULATION

In our experiment, we collect photons only from a section of the beam approximately one Rayleigh range z_0 in length, which includes the high-intensity region completely and cuts off the vast majority of the ionized volumes. The collection volume is depicted in Fig. 8. Most of the redshifted signal from the high-intensity region is imaged into a 105 μm core optical fiber with gold cladding to shield from noise. The one-to-one imaging system subtends 0.2 sr. The ionized volume that is captured by this imaging system is only about 10 times larger than the relevant high-intensity volume.

To simulate the entire expected signal for this experiment, we randomly distribute donor helium atoms throughout the imaged region of the focus at a pressure of 5×10^{-5} Torr. We compute the trajectories for the many electrons and calculate the in-band signal expected from this distribution. The simulation was repeated and averaged. Figure 9 shows the result as a function of peak laser intensity, assuming a constant beam waist of $w_0 = 6\lambda_L$, an imaging system that collects 0.2 sr of solid angle, and a 5% detection efficiency.

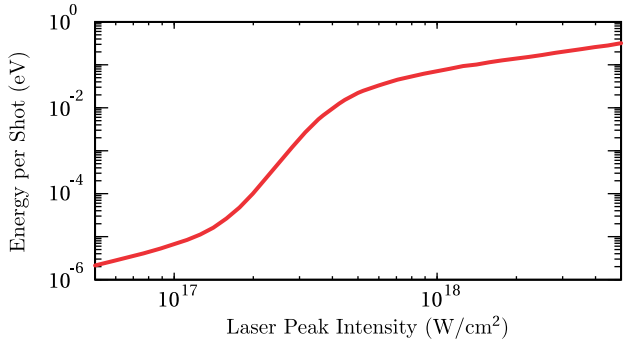

Fig. 9. Computed total energy per shot collected by the imaging system illustrated in Fig. 6 for varying peak intensities of the laser pulse. The beam waist is held fixed at $w_0 = 6\lambda_L$.

The redshifted signal "turns on" at intensities between 2×10^{17} W/cm^2 and 5×10^{17} W/cm^2. Below 10^{17} W/cm^2, the contribution from the ionization process is apparent. At higher intensities, the primary signal is from redshifted electrons, while the ionization effect contributes at the 1% level. Increasing the peak laser intensity above 10^{18} W/cm^2 only gradually increases the radiated energy emitted into the target-band region, owing in part to a tendency for the radiation to shift spatially towards the forward direction as the intensity increases. For a peak intensity of 2×10^{18} W/cm^2, the expected energy detected is 0.1 eV or about one photon per 14 shots. This is less than the estimate in Section 9 because the imaging system misses some of the high-intensity region as well as clips out most of the ionizing volume.

11. CONCLUSION

We simulated classical point-charge electron trajectories in a vector representation of a focused high-intensity laser pulse and calculated the scattered Thomson radiation out the side of the laser focus. Electrons that experience intensities near or above 10^{18} W/cm^2 drift in the forward direction, causing the light scattered in this perpendicular direction to be redshifted. Our proposed experiment measures scattered light in the vicinity of 900 nm, whereas the incident 35 fs laser pulse is centered at 800 nm. This analysis suggests that the beam waist should be at least several wavelengths, say $w_0 = 6\lambda_L$, to enable electrons to experience the highest intensities in the center of the focus without being pushed away.

We calculated the effective volume of electron initial positions that ensure exposure to high intensity, which is significantly smaller than the actual volume enclosing that intensity. This effective volume is significantly narrower in the dimension of the linear laser polarization and skewed towards the upstream side along the laser axis. Critically, we provide an estimate of the absolute redshifted emission into a detection solid angle based on a helium pressure of 5×10^{-4} Torr, which donates the free electrons. At this pressure, the vast majority of free electrons in the focus will originate from helium rather than from highly ionized background molecules (at 10^{-8} Torr). At 5×10^{-4} Torr, the emission in the perpendicular direction sums incoherently (i.e., intensities are added). For an assumed 5% detection efficiency, the estimate yields a photon count rate around one photon per 14 laser shots the peak intensity near 2×10^{18} W/cm^2. We computed this number as a function of laser intensity and found that higher intensities only marginally increase the yield, while somewhat lower intensities (down to 5×10^{17} W/cm^2) are also viable. Our estimates suggest that redshifted emission associated with the helium-ionization process is sufficiently weak to ignore when only the center part of the focus is imaged into the detector.

The emission rate predicted by QED is similar in strength to that predicted by the classical point emitters computed here, regardless of the size of the actual quantum wave packet. It appears feasible to liberate the electrons in the center of the laser focus using a prepulse arriving 100–200 fs prior to ensure that electron wave packets have the opportunity to expand to the size of a laser wavelength. Varying the delay of the prepulse would allow an experimental check as to whether the wave packet size has an impact on the emission rate. A first-quantized analysis would suggest that the scattered emission rate from large wave packets would be less by a couple of orders of magnitude.

ACKNOWLEDGMENTS

This work was supported by the National Science Foundation (Grant No. PHY-0970065).

REFERENCES

1. Y. I. Salamin, S. X. Hu, K. Hatsagortsyan, and C. H. Keitel, "Relativistic high-power lasermatter interactions," Phys. Rep. **427**, 41–155 (2006).
2. G. A. Mourou, T. Tajima, and S. V. Bulanov, "Optics in the relativistic regime," Rev. Mod. Phys. **78**, 309–371 (2006).
3. C. I. Moore, J. P. Knauer, and D. D. Meyerhofer, "Observation of the transition from Thomson to Compton scattering in multiphoton interactions with low-energy electrons," Phys. Rev. Lett. **74**, 2439–2442 (1995).
4. N. D. Powers, I. Ghebregziabher, G. Golovin, C. Liu, S. Chen, S. Banerjee, J. Zhang, and D. P. Umstadter, "Quasi-monoenergetic and tunable x-rays from a laser-driven Compton light source," Nat. Photonics **8**, 28–31 (2014).
5. X. Wang, R. Zgadzaj, N. Fazel, Z. Li, S. A. Yi, X. Zhang, W. Henderson, Y.-Y. Chang, R. Korzekwa, H.-E. Tsai, C.-H. Pai, H. Quevedo, G. Dyer, E. Gaul, M. Martinez, A. C. Bernstein, T. Borger, M. Spinks, M. Donovan, V. Khudik, G. Shvets, T. Ditmire, and M. C. Downer, "Quasi-monoenergetic laser-plasma acceleration of electrons to 2 GeV," Nat. Commun. **4**, 1988 (2013).
6. W. P. Leemans, B. Nagler, A. J. Gonsalves, C. Toth, K. Nakamura, C. G. R. Geddes, E. Esarey, C. B. Schroeder, and S. M. Hooker, "GeV electron beams from a centimetre-scale accelerator," Nat. Phys. **2**, 696–699 (2006).
7. E. Esarey, S. K. Ride, and P. Sprangle, "Nonlinear Thomson scattering of intense laser pulses from beams and plasmas," Phys. Rev. E **48**, 3003–3021 (1993).
8. K. Ta Phuoc, A. Rousse, M. Pittman, J. P. Rousseau, V. Malka, S. Fritzler, D. Umstadter, and D. Hulin, "X-ray radiation from nonlinear Thomson scattering of an intense femtosecond laser on relativistic electrons in a helium plasma," Phys. Rev. Lett. **91**, 195001 (2003).
9. J. S. Román, L. Roso, and H. R. Reiss, "Evolution of a relativistic wavepacket describing a free electron in a very intense laser field," J. Phys. B **33**, 1869–1880 (2000).
10. A. Galkin, A. Galstyan, V. Korobkin, M. Romanovskii, and O. Shiryaev, "Charged particle motion in the field of a short laser pulse of relativistic intensity," Bull. Lebedev Phys. Inst. **34**, 84–89 (2007).
11. J. Peatross, C. Müller, and C. H. Keitel, "Electron wavepacket dynamics in a relativistic electromagnetic field: 3-D analytical approximation," Opt. Express **15**, 6053–6061 (2007).
12. J. Gao, "Thomson scattering from ultrashort and ultraintense laser pulses," Phys. Rev. Lett. **93**, 243001 (2004).
13. E. A. Chowdhury, I. Ghebregziabiher, and B. C. Walker, "Larmor radiation from the ultra-intense field ionization of atoms," J. Phys. B **38**, 517–524 (2005).
14. G. R. Mocken and C. H. Keitel, "Radiation spectra of laser-driven quantum relativistic electrons," Comput. Phys. Commun. **166**, 171–190 (2005).
15. J. Peatross, C. Müller, K. Z. Hatsagortsyan, and C. H. Keitel, "Photo-emission of a single-electron wave-packet in a strong laser field," Phys. Rev. Lett. **100**, 153601 (2008).
16. J. P. Corson, J. Peatross, C. Müller, and K. Z. Hatsagortsyan, "Scattering of intense laser radiation by a single-electron wave packet," Phys. Rev. A **84**, 053831 (2011).
17. J. P. Corson and J. Peatross, "Quantum-electrodynamic treatment of photoemission by a single-electron wave packet," Phys. Rev. A **84**, 053832 (2011).
18. J. Peatross, J. P. Corson, and G. Tarbox, "Classical connection between near-field interactions and far-field radiation and the relevance to quantum photoemission," Am. J. Phys. **81**, 351–358 (2013).

19. F. Mackenroth, A. Di Piazza, and C. H. Keitel, "Determining the carrier-envelope phase of intense few-cycle laser pulses," Phys. Rev. Lett. **105**, 063903 (2010).
20. E. Lotstedt and U. D. Jentschura, "Nonperturbative treatment of double Compton backscattering in intense laser fields," Phys. Rev. Lett. **103**, 110404 (2009).
21. D. J. Griffiths, *Introduction to Electrodynamics*, 4th ed. (Pearson, 2013).
22. J. L. Chaloupka and D. D. Meyerhofer, "Observation of electron trapping in an intense laser beam," Phys. Rev. Lett. **83**, 4538–4541 (1999).
23. N. E. Rehler and J. H. Eberly, "Superradiance," Phys. Rev. A **3**, 1735–1751 (1971).
24. S. Augst, D. Strickland, D. D. Meyerhofer, S. L. Chin, and J. H. Eberly, "Tunneling ionization of noble gases in a high-intensity laser field," Phys. Rev. Lett. **63**, 2212–2215 (1989).
25. P. J. Ho, R. Panfili, S. L. Haan, and J. H. Eberly, "Nonsequential double ionization as a completely classical photoelectric effect," Phys. Rev. Lett. **94**, 093002 (2005).
26. M. Ware, S. A. Glasgow, and J. Peatross, "Energy transport in linear dielectrics," Opt. Express **9**, 519–532 (2001).